



Base-Free Benzyl Alcohol Aerobic Oxidation Catalyzed by AuPdNPs Supported on SBA-15 and TiO₂/SBA-15 Mesoporous Materials

Jussara Morais da Silva¹ · Renilma Carvalho Sousa¹ · Jean Cláudio S. Costa¹ · Janildo Lopes Magalhães¹ · Geraldo E. Luz Jr.² · Carla Veronica Rodarte de Moura¹ · Edmilson Miranda de Moura¹

Received: 18 February 2021 / Accepted: 5 April 2021

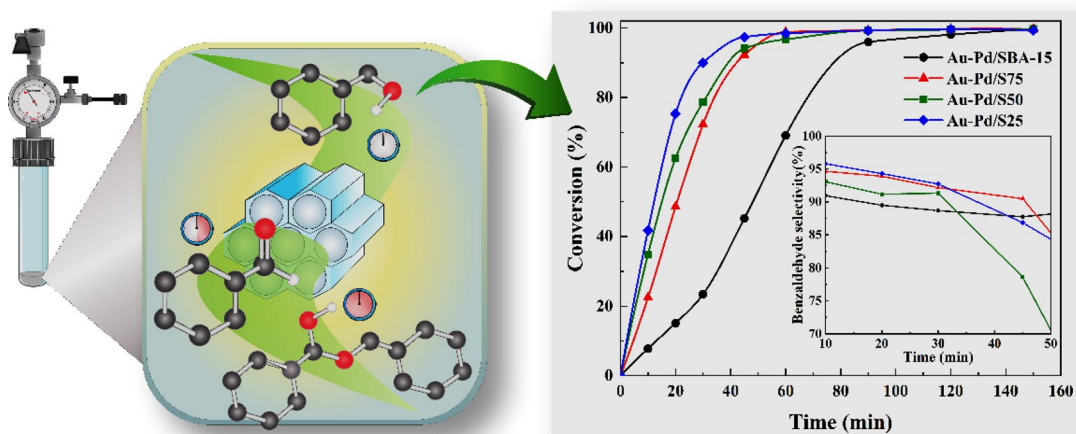
© The Author(s), under exclusive licence to Springer Science+Business Media, LLC, part of Springer Nature 2021

Abstract

It is known that the oxidative reactions of alcohols are sensitive to the characteristics of the catalyst, in such a way that the properties of the support are as important as those of the metallic phase. We consider the functionalization of support as a strategy to improve the catalytic performance in these reactions. We investigated the influence of the modification of the Si/Ti ratio of the TiO₂@SBA-15 support (RSi/Ti = 75, 50 and 25) on the catalytic performance of the synthesized materials: Me/SBA-15, Me/TiO₂@SBA-15 (Me = AuNPs or AuPdNPs). The techniques of XRD, adsorption, and desorption of N₂, ICP-OES, XPS, SEM, and TEM were used for characterization. The structure of the SBA-15 was maintained in all supports and catalysts and a significant reduction in particle size was observed in the modified support S25 (AuPd/SBA-15: 18.96 ± 12.48 nm; AuPd/S25 (RSi/Ti = 25): 3.14 ± 0.85 nm). All Au and AuPd catalysts performed well, showing activities > 53% in 2.5 h. However, bimetallic catalysts achieved greater prominence, reaching activities of 20 to 90% and selectivity > 90% for benzaldehyde in 0.5 h. Among them, the AuPd/S25 catalyst stood out with significant activity and selectivity (90%), in addition to good stability in successive reuse experiments.

Graphic Abstract

The TiO₂@SBA-15 support allows the synthesis of potentially active AuPd catalysts in aerobic oxidation of benzyl alcohol under base-free conditions and solvents.



Keywords SBA-15 · Functionalization · AuPdNPs · Catalysis · Oxidation

✉ Edmilson Miranda de Moura
 mmoura@ufpi.edu.br

Extended author information available on the last page of the article

1 Introduction

The oxidation of alcohols to their corresponding carboxylic acids and ketones is essential in synthetic organic chemistry [1–3]. The widespread use of these compounds as intermediates in the synthesis of products characteristic of fine chemistry (pharmaceuticals, food, and cosmetics) adds considerable economic value to them, increasing the industrial interest in high-efficiency processes.

Classic methods, based on potentially strong stoichiometric oxidants such as chromates and permanganates, provide high yields. However, the toxicity of the by-products and the risks offered during the processes evidenced the need for safer and environmentally acceptable methodologies, as guided by the principles of Green Chemistry proposed by Anastas and Kirchhoff [4].

Green Chemistry has a scope essentially based on safer processes and waste reduction. It is based on the efficient use of raw materials, preferably renewable, that reduce or eliminate residues and the use of toxic or dangerous reagents and solvents in their production and application [4, 5]. In the context of alcohol oxidation, catalysis presents itself as one of the essential tools for implementing Green Chemistry principles. It allows the use of less aggressive oxidants such as molecular oxygen and hydrogen peroxide, which produces only water as a byproduct [6, 7].

The combination of transition metals with molecular oxygen represents an alternative to standard oxidation processes. Heterogeneous catalysts based on supported Au and AuPd nanoparticles, for example, are active and selective in these processes and has been already well reported in the literature [8–11]. In Au's case, the process requires the addition of a base as a co-catalyst allowing the achievement of high activities. Although the base elevates the Au catalytic potential, its corrosive properties, and the residues generated in the processes negatively impact the industrial and environmental scope. It makes its use a limitation to the oxidation of alcohol [11–14].

AuPd bimetallic systems are more effective and fascinating since the synergism between metals overcomes these limitations and favors the metal-substrate interaction. These characteristics, combined with the support and the metal-support interaction properties, are considered determinant aspects of the catalytic potential of the material in the reaction, exhibiting significant effects, especially on selectivity.

Catalytic processes occur essentially on the catalyst's surface through simultaneous interactions of adsorption and desorption of reagents and products. In this aspect, in porous catalytic systems, the reagents' molecules diffuse through the pores to reach the entire surface. Whereas the molecules of the formed products need to leave, making

the active sites available for new adsorption. This mass transfer process depends heavily on the size, shape, and distribution of the material's pores [15]. Therefore, it is notable that porous catalysts tend to perform their activity better. In this context, SBA-15 mesoporous silica is attractive support due to its high specific surface area, wall thickness and adjusts orderly and well-defined pores. What motivates this study to strongly consider its use in the aerobic oxidation reactions of solvent-free and base benzyl alcohol [2, 16–21].

The low isoelectric point (IP) of silica (~ 2) confers some limitations to traditional synthesis methods, motivating studies to investigate and propose modifications of this material from the incorporation of transition metal oxides [20]. In a more recent study, Moreno-Martell et al. [21] reinforce the modification of SBA-15 as an alternative to change its isoelectric point, as well as other properties, enabling the incorporation of metallic nanoparticles by the traditional deposition–precipitation with urea method (DPU).

Among the proposals, TiO_2 and CeO_2 stand out for being reducible oxides capable of stabilizing metallic nanoparticles, storing and activating oxygen during the oxidation reactions, and providing high mobility to oxygen in the network [21–23]. Besides, the incorporation of TiO_2 promotes the addition of Brønsted acid-type active sites to SBA-15, inert support, free from active sites, whether acidic or basic [14, 23]. The characteristics mentioned make it possible for the TiO_2 /SBA-15 mesoporous material to directly participate in the reaction mechanism of oxidation, improving the catalyst's performance in the process [21].

Based on that, the present study reports the synthesis of heterogeneous catalysts by the DPU method, composed of AuNPs and AuPdNPs supported on SBA-15 and TiO_2 /SBA-15. The effects of the functionalization of the support were investigated, both in the structural, morphological, and textural properties and in the synthesized materials' catalytic performance.

2 Experimental Section

2.1 Materials

All chemicals used in the experiments were of analytical grade and were purchased commercially from Sigma-Aldrich, and no further purification was performed.

2.2 Synthesis of Supports

Mesoporous silicas of the SBA-15 type are commonly produced using the hydrothermal synthesis method, which may have some variations based on the procedure reported by Zhao et al. [24]. The procedure takes place in four stages:

(i) dissolution of the polymer; (ii) adding the silica source; (iii) aging; and (iv) heat treatment of drying and calcination. In the present study, we have been using the methodology reported by Araújo et al. [25], which reports both the synthesis of SBA-15 and SBA-15 modified with TiO_2 ($\text{TiO}_2/\text{SBA-15}$). The synthesis of TiO_2 nanocrystals in the form of colloidal suspension was later added to the synthesis of the SBA-15 matrix using in situ anchoring (ISA). The molar relations Si/Ti ($\text{RSi}/\text{Ti} = 75, 50, \text{ and } 25$) proposed in that work were also maintained.

2.3 Synthesis of Catalysts

Au and AuPd catalysts supported on SBA-15 and $\text{TiO}_2/\text{SBA-15}$ ($\text{R Si}/\text{Ti} = 75, 50, \text{ and } 25$) were synthesized by the DPU method, according to the procedure described below. In a round-bottom flask, 500 mg of support was added, followed by 50 ml of deionized water. The suspension was stirred at 800 rpm to disperse the support. Then, urea (99%) was added in a molar ratio of 100 to the metal [26–29]. After 5 min under constant agitation, the volume of a metal precursors solution corresponding to the metallic load of 2% (m/m) on the support was added. For this, $\text{HAuCl}_4 \cdot 3\text{H}_2\text{O}$ (30%) and PdCl_2 (99.9%) solutions were used in the concentration of $2.0 \text{ mmol} \cdot \text{L}^{-1}$. We use a molar ratio of 1:2 (Au: Pd) for bimetallic catalysts, keeping the total metallic load about 2% of the support. The system was kept constant agitation and gradual heating to 95°C ; the temperature was kept constant for 6 h. The obtained solids were separated by centrifugation and washed thoroughly with deionized water to remove the chloride ions. The materials were dried in the presence of air for 24 h at 100°C ; then they were calcined at 400°C for 6 h, under airflow with a heating rate of $10^\circ\text{C min}^{-1}$. Au, Pd, and AuPd catalysts supported on a TiO_2 were also synthesized to compare with the literature and other catalysts. All synthesized materials were coded according to their composition. The modified supports were named S75, S50, and S25, according to the molar ratio Si/Ti : 75, 50, and 25, respectively. The catalysts, in turn, were coded according to the general representation: metal/support.

2.4 Oxidation of Benzyl Alcohol

The catalysts' performance was verified using the oxidation of benzyl alcohol as a reaction model, which were carried out in a Fisher-Porter glass reactor with a capacity of 100 mL. The reactions were carried out on a magnetic stirrer coupled to a heated plate with temperature control. In a typical reaction, 1 ml (9.6 mmol) of benzyl alcohol and 28.5 mg (2% by weight of metal) of catalyst were added to the glass tube. For the tests with Au catalysts, the alkaline salt K_2CO_3 (99.95%) was added in a molar ratio of 80.5 (salt: metal) [30, 31]. The system containing the mixture was closed, purged,

and fed with oxygen gas up to a pressure of 4 bar. Then, it was kept under heating (100°C) and constant stirring for 2.5 h. After the determined time, the system was cooled, depressurized and the catalyst recovered by centrifugation. After separation, 20 μL of the reaction solution was diluted in 1 mL of methylene chloride (CH_2Cl_2) to determine the oxidation product's yields by gas chromatography (GC). The analyzes were performed using a GC-2010 Plus equipment (Shimadzu, Kyoto, Japan) equipped with a Carbowax capillary column and operating under conditions optimized to detect benzyl alcohol oxidation products (P-Xylene standard). The activity of the catalyst was measured by testing the conversion of benzyl alcohol and selectivity.

For the reuse test, the AuPd/S25 catalyst was subjected to successive reaction cycles. In each cycle, the reaction, centrifugation, removal of the reaction liquid, and the replacement of benzyl alcohol steps were performed. There were no washing steps between cycles.

2.5 Characterization of Materials

The structural aspects of the synthesized supports and catalysts were investigated by X-ray diffraction (XRD) using a Bruker D8 Advance diffractometer (Bruker AXS Gm6H, Karlsruhe, Germany) with $\text{CuK}\alpha$ radiation ($\lambda = 1.5406 \text{ nm}$). Data analysis was performed using the Rex 0.8.2 software [32] and was based only on identifying the phases present in the materials since the Rietveld refinement was disregarded due to the amorphous nature of SiO_2 . The textural properties were verified by the N_2 adsorption and desorption technique using ASAP-2420 equipment (Micromeritics, USA). For each analysis, an average of 93 mg of each previously degassed sample was used. The adsorption isotherms were obtained in a relative pressure range of 0.01 to 0.99 at a temperature of -196.15°C . The surface areas were estimated by the Brunauer–Emmett–Teller (BET) method and the pore volume distribution by the Barrett–Joyner–Halenda (BJH) method desorption branch of the isotherms. The catalysts' structural and morphological properties were verified using the scanning electron microscopy (SEM) and transmission electron microscopy (TEM) techniques. SEM images were obtained using a Quanta 200F FEG microscope and TEM images using a MORGAGNI 268D microscope (operating at 100 kV). For the TEM analysis, colloidal suspensions of the materials were prepared with isopropanol. The samples were deposited on a carbon-coated copper grid and dried under ambient conditions. The images obtained were analyzed with the aid of the ImageJ 1.52 software [33]. The average particle size and size distribution were verified considering 115 particles (average) for the AuPd/SBA-15 and AuPd/S25 materials and about 60 particles for the AuPd/S25 (R5) material. The pore size estimate was made in the same way, considering an average of 60 pores for the materials AuPd/

SBA-15 and AuPd/S25. The catalytic materials' elementary quantitative analysis was carried out in an inductively coupled plasma optical emission spectrometer (ICP-OES Radial) model Arcos (Spectro, Germany). The samples were prepared by the digestion procedure using nitric acid and hydrochloric acid in the proportion of 1:3 (HNO₃: HCl) under heating at 100 °C for 2 h. For each sample, 14 mg of catalyst were used. The surface chemical composition was verified by X-ray excited photoelectron spectroscopy (XPS) using a Scienta Omicron ESCA + spectrometer (Uppsala, Sweden) equipped with an EA 125 hemispherical analyzer and an XM 1000 monochrome X-ray source (Al K α , 1486, 7 eV). Data processing was performed using the Casa XPS® software. TA previous calibration of the spectra based on the C1s peak (BE = 284.8 eV) was performed to correct the charge accumulation. The peaks' adjustment was performed by applying Shirley-type background correction and then applying combined Gaussian and Lorentzian curves. For the quantitative analysis, the N_x atomic fractions of the interest elements were calculated from Eq. 1 [34, 35]. The operation was performed considering the correction of the areas (A_x) of the corresponding photoelectric peaks by applying the cross-section values (σ_x) calculated by Scofield [36].

$$\frac{N_A}{N_B} = \frac{A_A \times \sigma_B}{A_B \times \sigma_A} \quad (1)$$

3 Results and Discussion

3.1 Supports and Catalysts Characterization

For all samples (Fig. 1a), the patterns obtained exhibited three well-defined low-angle peaks located approximately 0.90°, 1.55°, and 1.80° (2 θ). The signals can be attributed to the reflections (100), (110), and (200), which are compatible

with the characteristic peaks of the hexagonal 2D ordering of cylindrical pores (symmetry P6mm). It indicates a well-ordered and defined mesoporous structure typical of materials of the type SBA-15 [24, 37].

Small displacements for lower value angles are observed in the modified support peaks to the SBA-15 matrix. These shifts indicate that the mesoporous parameters (α_0) increase concerning the matrix parameters (Table S1), which can be attributed to the incorporation of TiO₂ nanocrystals in the pure matrix [25]. The same displacement profile is observed in the catalysts' peaks, but the variations also occur concerning the respective supports. Therefore, similarly, this variation may be due to the impregnation of metallic nanoparticles [25].

In a medium angle, the XRD patterns showed for all supports (Fig. 1b) and catalysts (Fig. 1c) an intense and broad peak between 15° and 30° (2 θ), very characteristic of the amorphous silica that constitutes SBA-15. Among the supports and catalysts that contain TiO₂, only the patterns of the S25 support and the AuPd/S25 catalyst showed diffraction peaks corresponding to the reflections of the TiO₂ anatase phase planes (ICSD: 154602), confirming the presence of nanocrystals. The absence of these peaks in the patterns of other materials containing TiO₂ (S50, S75, AuPd/50, and AuPd/75) can be attributed to the low concentration of crystals SBA-15 matrix.

At a medium angle, the diffractograms of the catalysts (Fig. 1c) exhibit peaks consistent with the metallic phase of Au, more specifically with the reflections of the planes (111), (002), and (022) (ICSD: 44362). Peaks corresponding to the Pd metallic phase planes' reflections are not noticed in the crystallographic profiles of the catalysts. The signs are commonly displayed at around 39°, 45°, and 66° (2 θ), according to the crystallographic record (ICSD: 64914) indicated in Fig. 1c. However, the absence of these peaks does not exclude the presence of Pd in the samples. Factors such as low concentration, small particle size, and

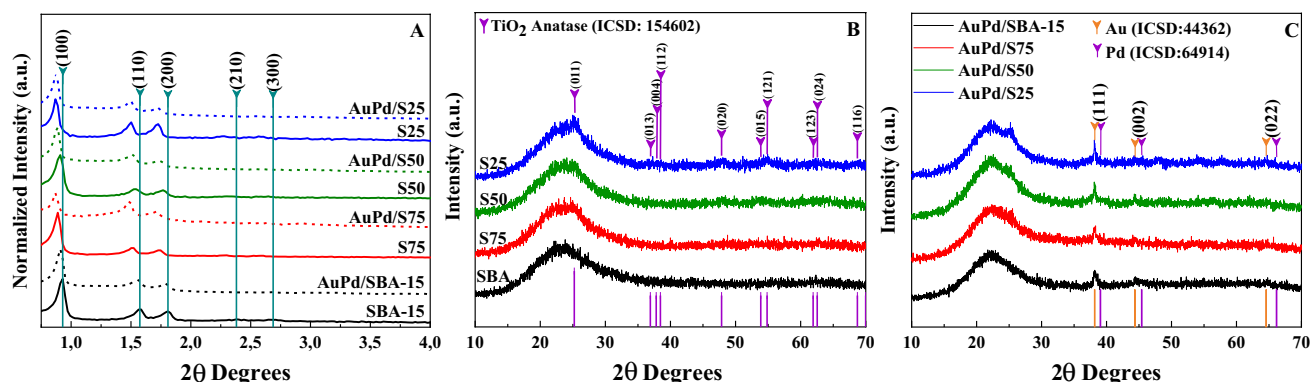


Fig. 1 X-ray diffractograms **a** of the supports and bimetallic catalysts (dashed line), **b** of the supports with different Si/Ti ratios, and **c** of the corresponding AuPd bimetallic catalysts

displacement due to the formation of metallic alloy with Au can contribute to a low definition of the corresponding peaks [38]. Besides, the ICP-OES and XPS techniques, which will be discussed later, clearly demonstrate Pd is presence in the addressed catalysts.

The isotherms of the supports and catalysts (Fig. 2) exhibit a characteristic profile of type IV isotherm (a) with an H1 type hysteresis loop [39]. Type IV (a) isotherms are typical of mesoporous materials with pores more massive than 4 nm, and the H1 type hysteresis loop is commonly found in materials that exhibit a narrow band of uniform cylindrical mesopores [21, 39, 40]. Both characteristics are according to the structure proposed by the diffractograms.

As expected, all synthesized substrates had a high specific surface area and high pore volume (Table S1). However, the values displayed by the supports containing TiO₂ were higher concerning the SBA-15. The observed increase can be attributed to the homogeneous distribution of the formed nanocrystals [25]. Especially the increase in the specific surface area, which may be due to the increase

in the roughness of the mesoporous walls due to the presence of TiO₂ nanocrystals [41].

As for the average pore diameter (Table S1), it is observed that there are no significant variations concerning SBA-15, suggesting the presence of TiO₂ nanocrystals on the walls of the SBA-15 matrix and that they do not obstruct the pores of the material. The results also show an increase in the modified materials' wall thickness, especially for the S25, indicating slightly higher hydrothermal stability and mechanical resistance compared to the others [20].

Mesoporous parameters (α_0) are calculated from information obtained in X-ray patterns and adsorption isotherms. The reflections observed in the diffractograms of porous materials at low angles are due to the difference in the electronic density between the pore walls and the empty spaces of the channels [42]. When incorporating particles in the mesoporous matrix occurs, the electronic density and in these spaces have interfered. This interference results in the displacement of the peaks to 2θ angles with smaller values and an increase in mesoporous parameters [25]. Peak shifts were confirmed by diffractograms

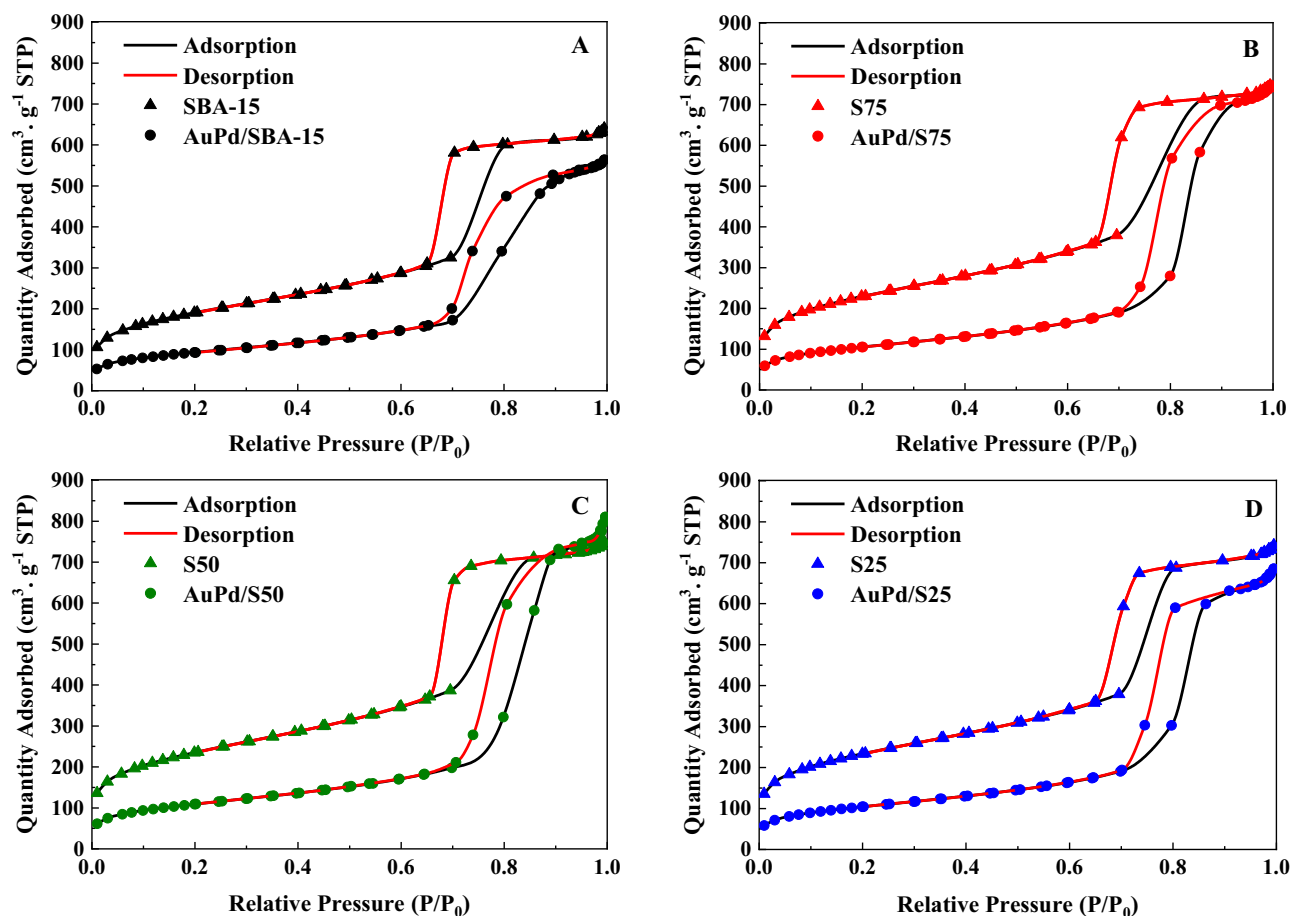


Fig. 2 N₂ adsorption and desorption isotherms from AuPd catalysts supported on SBA-15 and TiO₂@SBA-15 ($R_{Si/Ti}$ = 75, 50, and 25)

(Fig. 1a), and the values are shown in Table S1. Subtle increases were observed for the modified supports (S75, S50, and S25). The XRD results concerning peak displacement were observed in all catalysts, including those with TiO₂. This behavior was observed by the increase in the values of the mesoporous parameter compared to the corresponding supports' values.

The deposition of metals in the supports resulted in a marked reduction in the specific surface area and an increase in the average pore diameter. Both variations may be due to the agglomeration of metallic nanoparticles on the surface or in the silica mesopores, causing pore obstruction and the formation of interstitial pores. We believe that the interstices' presence interferes with the pore diameter calculation, justifying the increase in values and the broad size distributions observed in Figure S1.

In general, the data presented in Table S1 show that the addition of TiO₂ nanocrystals contributes to improving the textural properties of modified supports concerning SBA-15. As already mentioned, these properties can directly affect the catalytic performance of the materials. Therefore, the improvements presented in the properties suggest improvements in the catalysts' performance due to the addition of TiO₂.

Despite the advantages offered by the properties of SBA-15, studies report some limitations in the synthesis of catalysts by the most common methods and associate them mainly with the inert nature of SiO₂ [20, 43]. Thus, we verified the degree of deposition of the metallic content on the SBA-15 and S25 supports, which have a higher TiO₂ content.

The freshly prepared catalysts (AuPd/SBA-15 and AuPd/S25) were subjected to ICP-OES analysis to quantify the deposited metals. The results obtained (Table 1) indicate that the DPU procedure did not provide a complete metal deposition. However, the metallic content was satisfactory and expressive in both catalysts. The analysis also verified the real proportion of the metals and the individual quantities deposited, calculated according to the amount of precursor provided in the synthesis.

The results revealed a slightly higher metallic content for the AuPd/S25 catalyst and that this increase is mainly due to the more significant Au deposition compared to SBA-15. The greater deposition in the modified support can be related to improving the interaction of metals with the support surface. Since the low isoelectric point of the silica (~ 2) makes the surface negatively charged in an alkaline medium and does not favor metal ions' adsorption by the DPU method. It is, therefore, assumed that the addition of TiO₂ nanocrystals (PCZ ~ 6) increased the isoelectric point, promoting an improvement in ion adsorption [18, 21, 44, 45].

The newly prepared AuPd/SBA-15 and AuPd/S25 catalysts showed higher Au:Pd ratio values than the expected theoretical value, suggesting that the deposition was more effective for Au than for Pd. This characteristic is very well evidenced by the percentage of individual deposition, which indicates a more significant deposition of Au in both materials. The values suggest that TiO₂ favors the Au deposition mechanism and that the Pd deposition does not seem to be significantly influenced. Given these considerations, the mechanisms of deposition of Au and Pd in the supports may be different or competitive. Thus, Pd's incomplete deposition may be due to some factor to be adjusted in the synthesis, requiring more targeted studies.

The composition of the AuPd/S25 catalyst after reuse was also verified. The results show a lower metal content concerning the freshly prepared material, indicating leaching of some metals during the cycles. The sharp increase in the Au:Pd ratio indicates a more marked loss of Pd. This loss was confirmed by the amount of Pd (28%) and Au (0.4%) lost after reuse.

The morphological properties of the supports and catalysts were investigated by SEM and TEM. The images of the AuPd/SBA-15 and AuPd/S25 catalysts obtained by SEM (Figure S2A and Figure S2B) indicate that the supports are arranged in the form of short rods, demonstrating consistency with the literature [46, 47]. Besides, in both images, particles can be observed on the surface of the supports. Some particles are shown in Figure S2A show to be slightly larger than the particles shown in Figure S2B, probably due

Table 1 Quantification of the metallic composition of the newly prepared AuPd/SBA-15 and AuPd/S25 catalysts

Catalyst	Metal content (wt%)	Ratio Au/Pd (mol/mol)	Composition		Deposition		Loss	
			%Au	%Pd	%Au	%Pd	%Au	%Pd
Theoretical value	2.00	0.50	48.00	52.00	–	–	–	–
AuPd/SBA-15 ^a	1.43	0.68	55.91	44.09	82.90	60.62	–	–
AuPd/S25 ^a	1.52	0.86	61.56	38.44	97.14	56.91	–	–
AuPd/S25(R) ^b	1.35	1.20	68.89	31.11	–	–	0.39 ^c	27.97 ^c

^aClean catalysts

^bReused catalyst

^cValues calculated concerning the clean catalyst from the expression: $\text{Loss (\%)} = \left(1 - \frac{(\% \text{ Me} \times \text{Metal Content})^{[b]}}{(\% \text{ Me} \times \text{Metal Content})^{[a]}}\right) \times 100$

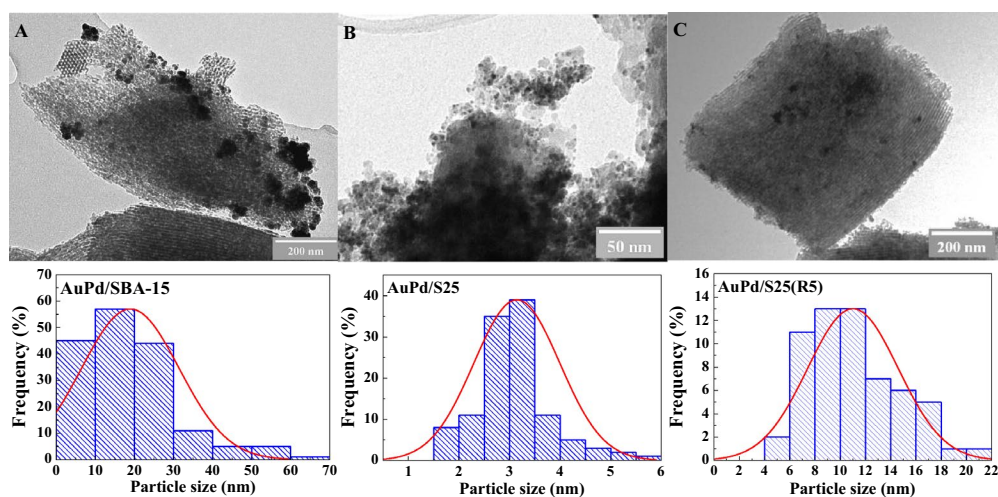


Fig. 3 Analysis of the size and dispersion of metallic nanoparticles in the catalysts **a** AuPd/SBA-15 and **b** AuPd/S25 before reuse and **c** AuPd/S25 after the 5th reaction cycle

to smaller particles' agglomeration. This condition is evidenced in the TEM images shown in Fig. 3.

TEM images (Figure S3) allow a more detailed visualization of the material and illustrate the mesopores in the form of long cylindrical channels and their hexagonal ordering, maintained in the catalysts. From the TEM images, it is also possible to confirm the presence of TiO_2 nanocrystals as a support modifier. As Figure S3B illustrates, small particles are displayed scattered over the matrix, while in Figure S3A no particles are observed. Similar results were obtained by Araújo et al. [25], confirming that the particles observed in the support are TiO_2 nanocrystals. Such observations demonstrate coherence with the diffractograms previously discussed.

The average pore diameter was also estimated from the TEM images and is according to the values suggested by the adsorption isotherms. The average diameters obtained were 6.8 and 7.2 nm for the AuPd/SBA-15 and AuPd/S25 catalysts, respectively.

The images revealed the existence of relatively large nanoparticles in AuPd/SBA-15 (Fig. 3a) and with a wide distribution of diameters (18.96 ± 12.48 nm), concurring a lack of uniformity in sizes, probably due to the agglomeration of smaller particles. In contrast, significantly small and dispersed nanoparticles were displayed in AuPd/S25 (Fig. 3b), where the narrow distribution of diameters (3.14 ± 0.85 nm) demonstrates the formation of particles with good uniformity. In a recent study, Rodríguez-Gómez et al. [38] report similar results for AuPd nanoparticles supported on SBA-15 and functionalized SBA-15, including highlighting a wider distribution for particles supported on SBA-15.

It is assumed that the particle agglomerations observed in the AuPd/SBA-15 catalyst are due to the weak interactions

between the metals and the support surface. As the interactions are weak, an occasional migration from smaller particles to larger particles may occur when the catalyst is subjected to heat treatments, mainly calcination [48]. In this context, the broad particle size distribution and its low dispersion can also be justified.

The narrow particle size distribution displayed on the AuPd/S25 catalyst suggests stronger interactions between the metals and the modified support. The stronger interactions indicate that the functionalization of SBA-15 with TiO_2 favors the dispersion of stabilized nanoparticles, allowing their formation in tiny sizes. This observation is in line with the proposal by Peza-Ladesma et al. [20] and Kučerová et al. [45]. Also, the improvements achieved with the modification of the support can be associated with factors such as the increase in acidity given to the material, a property that can contribute to the better dispersion of the particles [17], and the ability of TiO_2 to induce electronic effects that improve thermal stability, reducing sintering [20]. As for the reused catalyst (Fig. 3c), some changes are observed regarding the particles' size and distribution. These changes may represent evidence of leaching and sintering and will be discussed later.

The surface chemical composition of the AuPd/S25 catalyst was verified by the XPS technique to identify the chemical states of the elements available on its surface. The spectrum (Figure S4) indicates Au, C, O, Pd, Si, and Ti, as expected. Besides, there is no evidence of peaks corresponding to chlorine (~ 199.0 eV), indicating that the washing of the catalyst was efficient in removing the Cl^- ions from the metal precursors. In the Au 4f region (Fig. 4a) spectrum, the peaks' deconvolution showed two pairs of spin-orbit components ($\text{Au } 4f_{7/2}$ and $\text{Au } 4f_{5/2}$), indicating the contribution of two chemical species. The main deconvolution showed an

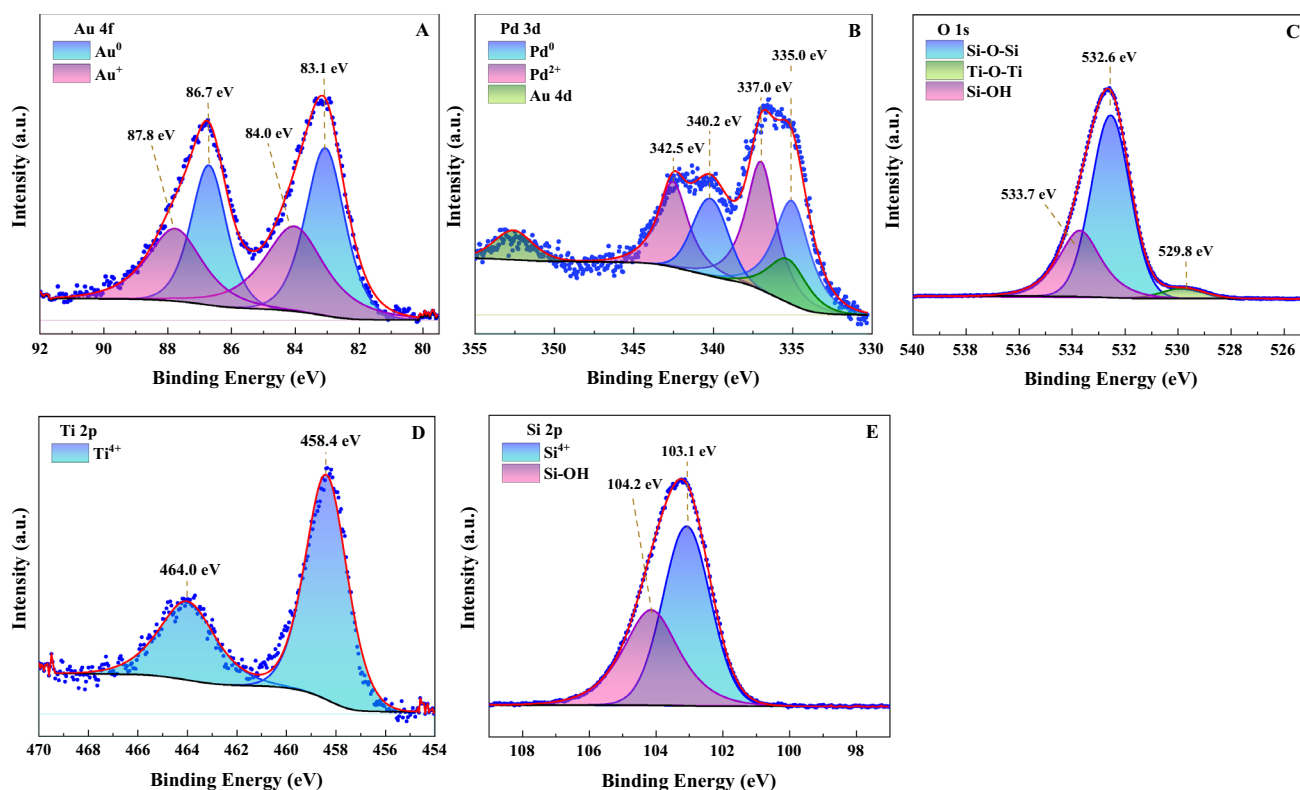


Fig. 4 High resolution XPS spectra of regions **a** Au 4f, **b** Pd 3d, **c** O 1s, **d** Ti 2p and **e** Si 2p of catalyst AuPd/S25

Au 4f_{7/2} peak at 83.1 eV attributed to the Au⁰ species. The respective value demonstrates a negative variation (−0.7 eV) of the binding energy concerning the characteristic value of metallic gold (83.8 eV) [49, 50].

The second doublet's deconvolution showed an Au 4f_{7/2} peak at 84.0 eV, which can be attributed to the Au⁺ species. The proximity of this value to 83.8 eV allows a consistent association with the proposal of authors such as Odio et al. [49], who attribute the formation of the Au⁺ species to the final state's effects. According to these authors, these effects are directly associated with the particles' size because, in tiny aggregates of Au⁰, the final state's effects would result in a positive net charge on the particle. It justifies the variation (+0.2 eV) in the binding energy of the Au metallic peak.

Like the Au 4f orbital, the deconvolution of the Pd 3d region (Fig. 4b) suggests two chemical species' contributions. Two pairs of spin–orbit components (Pd 3d_{5/2} and Pd 3d_{3/2}) are displayed with Pd 3d_{5/2} peaks at 335.0 eV, and 337.0 eV can be associated with the species Pd⁰ and Pd²⁺, respectively [51]. The occurrence of the Pd²⁺ species in the indicated binding energy is consistent with the presence of PdO on the catalyst surface. For the Pd 3d region, the Au 4d orbital contribution with two spin–orbit components, of which the Au 4d_{5/2} component occurs overlapping the Pd 3d_{5/2} peak.

The spectrum of the Ti 2p region (Fig. 4d) shows two components centered on the values 458.4 eV (Ti 2p_{3/2}) and 464.0 eV (Ti 2p_{1/2}), which are compatible with the Ti⁴⁺ species [52, 53]. As for the Si 2p region (Fig. 4e), two intense contributions are observed in 103.1 eV and 104.2 eV. The contribution of less energy can be easily attributed to the Si⁴⁺ species, a characteristic peak of SiO₂. The one with the highest energy shows compatibility with Si–OH bonds, arising from the contribution of silanol groups and weakly adsorbed OH[−] species from some hydration [54, 55]. The deconvolution of the O 1s spectrum (Fig. 4c) exhibited three contributions, whose binding energies are attributed to the presence of Si–O–Si (532.6 eV), Ti–O–Ti (529.8 eV), and Si–OH (533.9 eV), in the latter case, as in the Si 2p region, the contribution of silanol groups and weakly adsorbed species is considered. All values presented demonstrate consistency with the literature [56].

As reported, a significant variation in the binding energy of the Au 4f_{7/2} peak is observed concerning the value commonly reported for Au⁰ (83.8 eV). This variation can be associated with electronic changes in Au resulting from the charge transfer between Pd, which indicates close interactions between Au and Pd atoms and mainly the formation of AuPd alloy [23, 57]. Given the magnitude of the variation, it is also possible that there is an influence of support effects, mainly due to interactions between Au and TiO₂ [23].

The atomic proportions between the reduced and oxidized Au species ($\text{Au}^0/\text{Au}^{\text{ox}}=0.85$) and Pd ($\text{Pd}^0/\text{Pd}^{\text{ox}}=1.12$) suggest an inevitable heterogeneity in the surface chemical composition of the catalyst. The Au 4f setting, as already mentioned, suggests the occurrence of the metallic phase in the alloy as AuPd and the form of segregated nanoparticles. The ratio obtained by adjusting the Pd 3d indicates the majority contribution (46.1%) of the Pd^{2+} species concerning the Pd^0 species (40.4%) in photoelectric spectra.

The presence of the oxidized species Pd^{2+} can be associated with the contribution of several factors, which involve characteristics of the synthesis method [58], presence of free Pd on the support surface, exposure to heat treatments [59], and effects of support, mainly due to the occurrence of electronic interactions [60]. In this context, the ability of TiO_2 to supply oxygen and the presence of oxygen vacancies can favor these interactions. This property of TiO_2 contributes relatively to the presence of Pd^{2+} on the surface of the catalyst [23, 53].

The quantitative results also indicated an Au/Pd atomic ratio of 0.66, lower than the molar ratio presented by the ICP-OES technique (0.86). This variation may suggest the occurrence of metal deposition inside the mesoporous system of the support, reflecting a lower concentration of metal on the surface [61].

3.2 Catalytic Activity

The functionalization of the SBA-15 was investigated from the catalysts' performance in the reaction of oxidation of benzyl alcohol without solvent addition in the presence of molecular oxygen as oxidant. The products that can be obtained by oxidation benzyl alcohol are shown in Scheme 1.

Initially, we verified the conversion of alcohol in the absence of catalyst through some blank tests, from which substrate oxidation was investigated under the

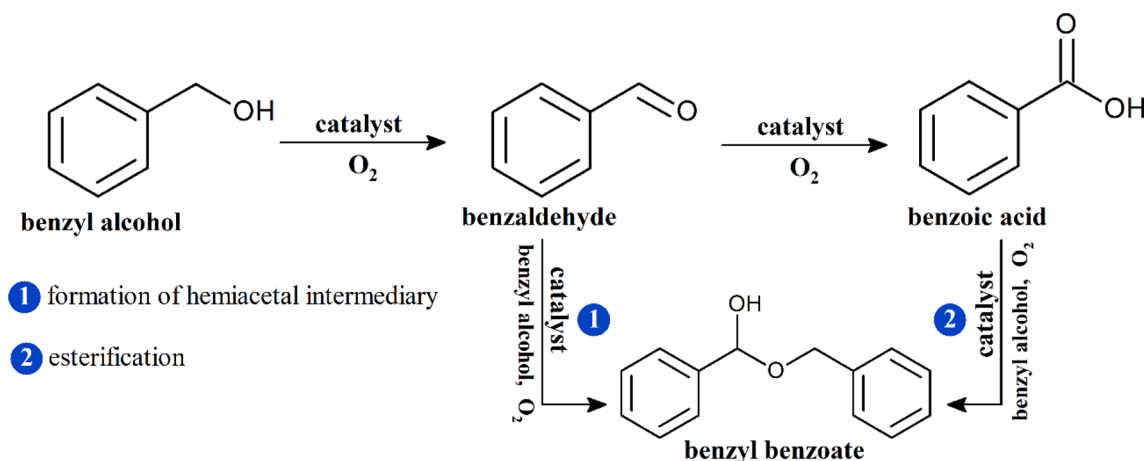
reaction conditions (Table S2, entry 2) and in their absence (Table S2, entry 1). The values obtained are within the considered error and have no catalytic relevance. The same is right for tests performed only in the supports' presence (Table S2, entries 3–7).

Since Au's low activity in the absence of base is very well established in the literature, we consider the addition of determining amounts of K_2CO_3 in the reactions [1, 14]. As expected, tests performed in the absence of K_2CO_3 showed shallow conversion of benzyl alcohol (Table S2, entries 8–12), while in the presence of salt, the activity of the catalysts increased considerably (Fig. 5a).

For AuPd catalysts (Fig. 5b), the tests were performed only in the absence of a base. The results obtained demonstrated maximum conversion of benzyl alcohol (99%) with selectivities distributed between the benzaldehyde (least oxidized product) and the benzyl benzoate. These results are consistent with the literature since Au catalysts showed activity only in the presence of a base and with lower performance than AuPd catalysts as expected [1, 11–14].

The inclusion of Pd to compose a bimetallic system next to Au is an alternative to the base's use. Synergism between the metals involved tends to contribute significantly to the catalytic performance, making the alkaline medium dispensable [8, 64]. Also, for Mallat and Baiker, Pd's addition can activate alcohol, accelerate the reaction rate, and promote changes in the distribution of products, improving selectivity [1]. The synergistic effect between metals is quite pronounced since the corresponding monometallic catalysts (Au/S25 and Pd/S25) did not show activity in the oxidation of benzyl alcohol under base-free conditions.

The results obtained with Au catalysts show an increasing trend associated with an increase in the amount of TiO_2 in the support. In the same sense, there is also a shift in selectivity in favor of benzoic acid. Such results



Scheme 1 Representation of products obtained by the oxidation of benzyl alcohol [62, 63]

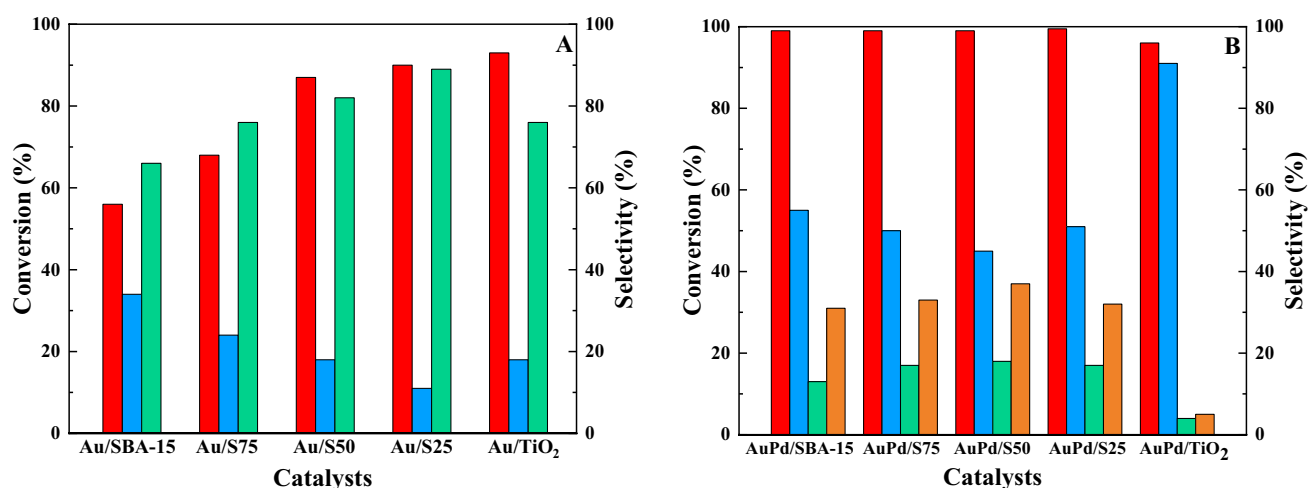


Fig. 5 Evaluation of the activity and selectivity of **a** Au catalysts in the presence of a base and **b** AuPd without the base in the oxidation of benzyl alcohol^a. Legend: Conversion (Filled circle Red), Benzaldehyde (Filled circle Blue), Benzoic acid (Filled circle green), Ben-

zyl benzoate (Filled circle Orange). ^aReaction conditions: 9.6 mmol of benzyl alcohol, 4.1 mmol of metal (catalyst), 4 bar of O₂, 100 °C, 2.5 h, 0.33 mmol of K₂CO₃, 600 rpm

suggest that the presence of TiO₂ nanocrystals acts on the performance of these catalysts.

The maximum conversion achieved by the bimetallic catalysts under the determined conditions does not allow to perceive any relationship between the catalytic performance and the functionalization of the support. According to the literature, the carboxylic acid and the ester are products of sequential reactions of the oxidation of alcohol, the acid is formed from the oxidation of the aldehyde [1, 14], and the ester from the esterification of the acid with

alcohol [62] or by the formation of a hemiacetal intermediate [63] (Scheme 1).

This proposal, combined with the remarkable amount of benzyl benzoate produced, suggests a strong dependence on selectivity as a function of reaction time. It is confirmed by the performance profiles shown in Fig. 6a.

The conversion profiles indicate catalytic activity for all materials in the initial 10 min of the process. Moreover, demonstrate greater activity for catalysts with modified support, as it occurs for Au catalysts. The optimal reaction time was fixed at 30 min since, in that time, the highest values

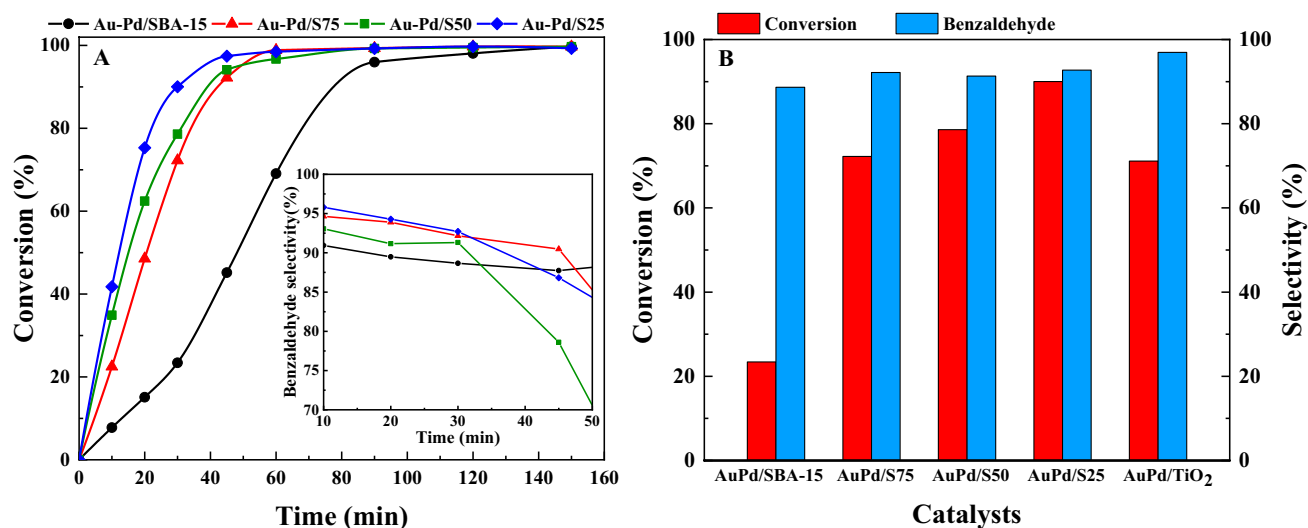


Fig. 6 **a** conversion and selectivity profiles as a function of time for bimetallic catalysts. ^a**b** evaluation of the potential of bimetallic catalysts in the oxidation of benzyl alcohol in the optimal time ^{a,b}. ^aReac-

tion conditions: 9.6 mmol of benzyl alcohol, 4.1 mmol of metal (catalyst), 4 bar of O₂, 100 °C. ^bOptimum time: 30 min

for conversion and selectivity are reached (Fig. 6). At the optimum time, all catalysts showed activity superior to that of AuPd/SBA-15 ($\text{Si/Ti}=0$) and the catalysts AuPd/S50 ($\text{Si/Ti}=50$) and AuPd/S25 ($\text{Si/Ti}=25$) obtained higher activity than AuPd/TiO₂. These results suggest a good combination between SBA-15 and TiO₂ and show a direct relationship between increased catalytic activity and the presence of TiO₂ in the support.

3.3 Selectivity Study

Regardless of the support, all Au catalysts achieved expressive selectivities (60–80%) for benzoic acid. Studies suggest that the alkaline pH favors the deprotonation of alcohol and hydration of the aldehyde, increasing the reaction rate and gives rise to oxidation to the final product (carboxylic acid). The alkaline medium also helps in the desorption of benzoic acid, favoring its selectivity [1, 14].

For evaluating the selectivity profile of bimetallic catalysts, only the results of the best performing catalyst were considered: AuPd/S25. The selectivity for benzaldehyde was extremely significant, especially in the optimal reaction time (30 min). The formation of appropriate amounts of benzoic acid and benzyl benzoate are observed as the reaction time increases (Figure S5). The formation of these co-products, mainly of the ester, may be related to the acidity of the catalyst [8, 14, 65].

The formation of benzoic acid is observed after 10 min of reaction and does not show significant variation after 45 min. On the other hand, benzyl benzoate formation is observed only after 45 min, presenting an increasing profile. Comparing the curves corresponding to benzaldehyde and benzyl benzoate, we note similarities in the two profiles' variation. Such variations suggest an inverse relationship in forming the two products, where benzaldehyde is consumed as benzyl benzoate is produced. Therefore, benzyl benzoate can be produced from a hemiacetal intermediate formed by hydrogenation of benzaldehyde, as proposed by Cao et al. [65] and Enache et al. [63].

3.4 Influence of Temperature and Pressure

The influence of pressure and temperature conditions was verified considering a temperature range of 80 °C to 120 °C and inlet pressures of 3, 4, and 5 bar (Table S3). The increase in temperature improved the conversion but reduced the selectivity for benzaldehyde. Similarly, the increase in pressure also positively affected the conversion and decreased selectivity, although with more subtle variations. Thus, the data presented suggest an opposite dependence on benzaldehyde's selectivity concerning the increase in temperature and pressure.

The selectivity of benzoic acid and benzyl benzoate increases with temperature, reaching a significant change at 120 °C. This behavior is also shown with increased pressure, but more subtly. When the pressure is increased from 3 to 5 bar at 100 °C, a positive variation in benzoic acid and benzyl benzoate selectivities is observed. A positive variation is also observed for benzaldehyde, but only in the change from 3 to 4 bar. Cao et al. [66] observed such trends due to the greater availability of O₂ on the catalyst's surface. The pressure increase raises the O₂ concentration in the reaction.

The negative variation observed in the benzaldehyde selectivity when the pressure supplied is 5 bar may be due to the oxidation of the benzaldehyde itself since more benzoic acid and benzyl benzoate are produced. The results obtained at 4 bar point to the reaction's saturation, indicating that, from there, the reaction tends to proceed for the more oxidized products. Therefore, it is consistent to consider the temperature of 100 °C and the inlet pressure of 4 bar as optimal conditions for the reaction.

3.5 Effects of Modifying SBA-15 on Catalyst Performance

As it has already been mentioned, the application of SBA-15 as catalytic support is attractive because of the unique double porosity system and its high specific surface area. The inert nature of SiO₂ underlies the approach to the functionalization of SBA-15 with organic groups, transition metals, and transition metal oxides in search of improvement, both in terms of material properties and in the interactions between support, active phase, and substrate.

The use of TiO₂ as a modifier of SBA-15 is opportune due to its complete application as catalytic support, especially in systems based on AuNPs and AuPdNPs, and the emphasis is given to its properties against oxidative processes. Thus, the present study was based on obtaining an improved catalytic system by combining the two materials' properties. That is, a system that maintains the structural and morphological characteristics of silica and that shows the physical–chemical and catalytic properties of TiO₂.

In the verification of the catalytic performance, the results obtained demonstrated that all catalysts (Au and AuPd) with modified support (TiO₂@SBA-15) presented superior performance to the catalysts with unmodified support (SBA-15). Besides, the increasing activity profile observed exposed a direct relationship between the activity and the Si/Ti molar ratio of the support, so that more significant catalytic activities were achieved with the increase in the amount of TiO₂.

Among the bimetallic catalysts, the material AuPd/S25 ($R_{\text{Si/Ti}}=25$) was considered the most effective, while the catalyst AuPd/SBA-15 ($R_{\text{Si/Ti}}=0$) was the least active. Knowing that the oxidation of benzyl alcohol is a process sensitive to the properties of the catalyst, the investigation

of the structural morphological and textural aspects of these materials is crucial in understanding the role of TiO_2 in its performance.

The properties of SBA-15 were shown by all the characterization techniques used, XRD, SEM, and TEM images, adsorption isotherms. The properties were observed in all catalysts, regardless of the amount of TiO_2 and the metallic particles' addition. However, as already noted, the nanoparticles' placement on the supports was different in terms of size and dispersion. While AuPd/SBA-15 exhibited the formation of relatively large particle clusters (20 nm), AuPd/S25 exhibited considerably smaller average particle size (~ 3 nm), besides too good dispersion.

Based on these observations, the marked variation in activity between the AuPd/SBA-15 and AuPd/S25 catalysts can be firmly attributed to the differences in the size and dispersion of the metallic nanoparticles in each support. These characteristics are associated with the presence of TiO_2 . Considering that the addition of this oxide as an SBA-15 modifier possibly favored the establishment of more robust interactions between the metals and the support, improving dispersion and reducing the size of the particles.

The occurrence of an increase in the activity profile demonstrated by the catalysts AuPd/S75, AuPd/S50, and AuPd/S25 (in that order), together with the catalytic properties and the favorable aspects to oxidation that are commonly reported, allow the hypothesis of direct participation of TiO_2 in the oxidative mechanism of benzyl alcohol. Therefore, a more detailed study of the reaction mechanism involved in the process is relevant.

3.6 AuPd/S25 Catalyst Reuse Test

The reduction in catalyst performance is commonly associated with factors such as leaching, sintering, and poisoning. The contribution of the factors is related to the properties of the catalytic material. This fact requires the investigation of each one.

After completing the five reaction cycles, the catalyst was subjected to TEM and ICP-OES analyzes. The images obtained by TEM (Fig. 3c) showed an increase in the average particle diameter concerning the newly prepared catalyst. Particles with about 11.0 nm were observed, indicating a certain degree of agglomeration and sintering. Besides, there is an apparent reduction in the particles' dispersion, which suggests loss of metallic content and less availability of active sites. Therefore, although sintering contributes to the loss of activity, it cannot be considered the most outstanding contribution, much less the determining factor (Fig. 7).

Previously, we discussed that the loss of the catalyst's active phase, after reuse, was verified by ICP-OES. The results obtained and presented in Table 2 indicated a loss of

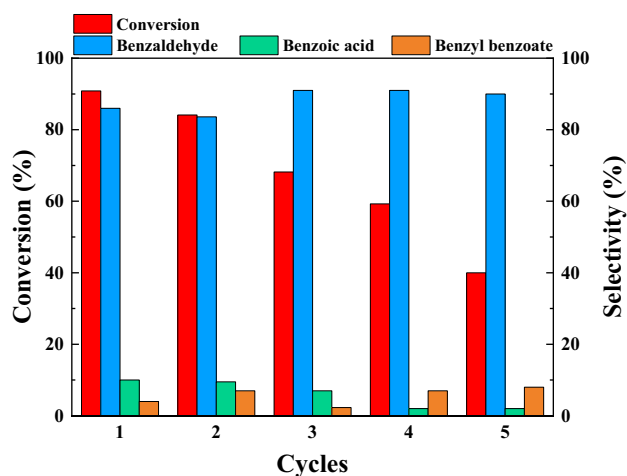


Fig. 7 Evaluation of the recycling of the AuPd/S25 catalyst in the oxidation of benzyl alcohol in the absence of washing steps

11.2% of the metallic content concerning the newly prepared catalyst, confirming the occurrence of leaching. Besides, the analysis also made it possible to verify that there was a significant loss of Pd: 28%, which represents $\sim 98\%$ of the total leached metallic content.

The more significant Pd loss concerning Au can consistently justify the reduction of the catalytic potential throughout the cycles. Since, under basic conditions, the AuPd synergism is what gives activity to the system. The results shown demonstrate consistency with that reported by Wang et al. [67]. Based on similar observations, the authors attribute the drop-in activity to the lack of homogeneity of Pd on the particles' surface. This characteristic, combined with segregation, weakens the synergistic effects of bimetallic catalysts without affecting selectivity, just as it does for the AuPd/S25 catalyst [67].

About catalyst poisoning, there is the possibility of blocking the active sites due to the strong adsorption of molecules from the substrate and products, especially carboxylic acid [68]. However, as leaching is a factor that significantly affects catalysis, the study of the occurrence of catalyst poisoning was not considered.

4 Conclusion

The modification of SBA-15 by the addition of TiO_2 demonstrated positive effects on the Au and AuPd catalysts' performance. The AuPd catalysts, which were more efficient, were characterized by different techniques to guarantee the properties and composition of the support phase and investigate the metallic phase properties. Such techniques demonstrated improvements in the properties of the support and AuPdNPs due to the addition of TiO_2 . AuPd catalysts'

activities on different supports were studied in the oxidation of benzyl alcohol using molecular oxygen as an oxidant under solvent and base-free conditions. The catalysis results show an increase in activity, which is associated with an increase in the amount of TiO₂ in the support. The combination of these results shows the positive contribution of the modification of the SBA-15, exposes the possibility of direct participation of TiO₂ in the reaction mechanism, and establishes the AuPd/S25 catalyst as the most effective. Besides, experimental data suggested relevant effects of time, pressure, and temperature on catalytic performance. Moreover, among the conditions, time was the most significant effect of the production benzaldehyde. Thus, using the optimum conditions of 100 °C, 0.5 h and 4 bar, we verify the stability of the AuPd/S25 catalyst. The catalyst was used for five successive cycles in which it showed loss of activity, the most significant loss being in the last cycle. The catalyst showed no drop in selectivity but a slight increase from the third cycle. The loss of activity can be mainly associated with the loss of Pd during the reaction cycles. The catalyst could be used for five successive cycles without loss of selectivity and presented, in the last cycle, a conversion of 40%. These results represent good catalyst stability. The catalyst also offers a reasonable selectivity control, being able to be alternated between two main products, benzaldehyde, and benzyl benzoate, based on the variation of the reaction conditions, mainly over time.

Supplementary Information The online version contains supplementary material available at <https://doi.org/10.1007/s10562-021-03624-6>.

Acknowledgements The authors acknowledge financial support from FAPEPI and CNPq and the technical support of Center for Strategic Technology of the Northeast (CETENE-PE).

References


- Mallat T, Baiker A (2004) Oxidation of alcohols with molecular oxygen on solid catalysts. *Chem Rev* 104:3037–3058. <https://doi.org/10.1021/cr0200116>
- Chen Y, Li W, Wang J et al (2016) Gold nanoparticle-modified TiO₂/SBA-15 nanocomposites as active plasmonic photocatalysts for the selective oxidation of aromatic alcohols. *RSC Adv* 6:70352–70363. <https://doi.org/10.1039/c6ra11390g>
- Sheldon RA (2015) Recent advances in green catalytic oxidations of alcohols in aqueous media. *Catal Today* 247:4–13. <https://doi.org/10.1016/j.cattod.2014.08.024>
- Anastas PT, Kirchhoff MM (2002) Origins, current status, and future challenges of green chemistry. *AccChem Res* 35:686–694. <https://doi.org/10.1021/ar010065m>
- Sheldon RA (2000) Atom utilisation, E factors and the catalytic solution. *Comptes Rendus l'Academie des Sci - Ser IIc Chem* 3:541–551. [https://doi.org/10.1016/S1387-1609\(00\)01174-9](https://doi.org/10.1016/S1387-1609(00)01174-9)
- Anastas PT, Kirchhoff MM, Williamson TC (2001) Catalysis as a foundational pillar of green chemistry. *Appl Catal A Gen* 221:3–13. [https://doi.org/10.1016/S0926-860X\(01\)00793-1](https://doi.org/10.1016/S0926-860X(01)00793-1)
- Arends IWCE, Sheldon RA (2010) Modern oxidation of alcohols using environmentally benign oxidants. *Modern oxidation methods*. Wiley-VCH Verlag GmbH & Co. KGaA, Weinheim, Germany, pp 147–185
- Enache DI, Edwards JK, Landon P et al (2006) Solvent-free oxidation of primary alcohols to aldehydes using Au-Pd/TiO₂ catalyst. *Science* 311(80):362–365. <https://doi.org/10.1126/science.1120560>
- Haruta M (2002) Catalysis of gold nanoparticles deposited on metal oxides. *CATTECH* 6:102–115. <https://doi.org/10.1023/A:1020181423055>
- Haruta M, Kobayashi T, Sano H, Yamada N (1987) Novel gold catalysts for the oxidation of carbon monoxide at a temperature far below 0 °C. *Chem Lett* 16:405–408. <https://doi.org/10.1246/cl.1987.405>
- Prati L, Rossi M (1998) Gold on carbon as a new catalyst for selective liquid phase oxidation of diols. *J Catal* 176:552–560. <https://doi.org/10.1006/jcat.1998.2078>
- Porta F, Prati L, Rossi M et al (2000) Metal sols as a useful tool for heterogeneous gold catalyst preparation: reinvestigation of a liquid phase oxidation. *Catal Today* 61:165–172. [https://doi.org/10.1016/S0920-5861\(00\)00370-9](https://doi.org/10.1016/S0920-5861(00)00370-9)
- Prati L, Martra G (1999) New gold catalysts for liquid phase oxidation. *Gold Bull* 32:96–101. <https://doi.org/10.1007/BF03216617>
- Davis SE, Ide MS, Davis RJ (2013) Selective oxidation of alcohols and aldehydes over supported metal nanoparticles. *Green Chem* 15:17–45. <https://doi.org/10.1039/c2gc36441g>
- Leofanti G, Padovan M, Tozzola G, Venturelli B (1998) Surface area and pore texture of catalysts. *Catal Today* 41:207–219. [https://doi.org/10.1016/S0920-5861\(98\)00050-9](https://doi.org/10.1016/S0920-5861(98)00050-9)
- Kumar A, Kumar VP, Srikanth A et al (2016) Vapor phase oxidation of benzyl alcohol over nano Au/SBA-15 catalysts: effect of preparation methods. *Catal Lett* 146:35–46. <https://doi.org/10.1007/s10562-015-1656-7>
- Calzada LA, Castellanos R, García LA, Klimova TE (2019) TiO₂, SnO₂ and ZnO catalysts supported on mesoporous SBA-15 versus unsupported nanopowders in photocatalytic degradation of methylene blue. *Microporous Mesoporous Mater* 285:247–258. <https://doi.org/10.1016/j.micromeso.2019.05.015>
- Liotta LF, Pantaleo G, Puleo F, Venezia AM (2012) Au/CeO₂-SBA-15 catalysts for CO oxidation: effect of ceria loading on physico-chemical properties and catalytic performances. *Catal Today* 187:10–19. <https://doi.org/10.1016/j.cattod.2012.01.001>
- Chaudhary V, Sharma S (2017) An overview of ordered mesoporous material SBA-15: synthesis, functionalization and application in oxidation reactions. *J Porous Mater* 24:741–749. <https://doi.org/10.1007/s10934-016-0311-z>
- Peza-Ledesma CL, Escamilla-Perea L, Nava R et al (2010) Supported gold catalysts in SBA-15 modified with TiO₂ for oxidation of carbon monoxide. *Appl Catal A Gen* 375:37–48. <https://doi.org/10.1016/j.apcata.2009.12.009>
- Moreno-Martell A, Pawelec B, Nava R et al (2018) CO oxidation at 20 °C on Au catalysts supported on mesoporous silica: effects of support structural properties and modifiers. *Materials (Basel)*. <https://doi.org/10.3390/ma11060948>
- Schubert MM, Hackenberg S, Van Veen AC et al (2001) CO oxidation over supported gold catalysts - "Inert" and "active" support materials and their role for the oxygen supply during reaction. *J Catal* 197:113–122. <https://doi.org/10.1006/jcat.2000.3069>
- Khawaji M, Chadwick D (2018) Au-Pd NPs immobilised on nanostructured ceria and Titania: impact of support morphology on the catalytic activity for selective oxidation. *CatalSci Technol* 8:2529–2539. <https://doi.org/10.1039/c7cy02329d>
- Zhao J, Huo Q, Melosh N et al (1998) Triblock copolymer syntheses of mesoporous silica with periodic 50 to 300 angstrom

- pores. *Science* 279(80):548–552. <https://doi.org/10.1126/science.279.5350.548>
25. Araújo MM, Silva LKR, Sczancoski JC et al (2016) Anatase TiO₂ nanocrystals anchored at inside of SBA-15 mesopores and their optical behavior. *Appl Surf Sci* 389:1137–1147. <https://doi.org/10.1016/j.apsusc.2016.08.018>
 26. Lu X, Zhao G, Lu Y (2013) Propylene epoxidation with O₂ and H₂: a high-performance Au/TS-1 catalyst prepared via a deposition-precipitation method using urea. *CatalSciTechnol* 3:2906–2909. <https://doi.org/10.1039/c3cy00339f>
 27. Delannoy L, Thrimurthulu G, Reddy PS et al (2014) Selective hydrogenation of butadiene over TiO₂ supported copper, gold and gold-copper catalysts prepared by deposition-precipitation. *PhysChemChemPhys* 16:26514–26527. <https://doi.org/10.1039/c4cp02141j>
 28. Zanella R, Delannoy L, Louis C (2005) Mechanism of deposition of gold precursors onto TiO₂ during the preparation by cation adsorption and deposition-precipitation with NaOH and urea. *ApplCatalA Gen* 291:62–72. <https://doi.org/10.1016/j.apcata.2005.02.045>
 29. Zanella R, Giorgio S, Henry CR, Louis C (2002) Alternative methods for the preparation of gold nanoparticles supported on TiO₂. *J PhysChem B* 106:7634–7642. <https://doi.org/10.1021/jp0144810>
 30. De Abreu WC, Garcia MAS, Nicolodi S et al (2018) Magnesium surface enrichment of CoFe₂O₄ magnetic nanoparticles immobilized with gold: reusable catalysts for green oxidation of benzyl alcohol. *RSC Adv* 8:3903–3909. <https://doi.org/10.1039/c7ra13590d>
 31. Gualteros JAD, Garcia MAS, da Silva AGM et al (2019) Synthesis of highly dispersed gold nanoparticles on Al₂O₃, SiO₂, and TiO₂ for the solvent-free oxidation of benzyl alcohol under low metal loadings. *J Mater Sci* 54:238–251. <https://doi.org/10.1007/s10853-018-2827-x>
 32. Bortolotti M, Lutterotti L, Lonardelli I (2009) ReX: a computer program for structural analysis using powder diffraction data. *J ApplCrystallogr* 42:538–539. <https://doi.org/10.1107/S0021889809008309>
 33. Schindelin J, Arganda-Carreras I, Frise E et al (2012) Fiji: an open-source platform for biological-image analysis. *Nat Methods* 9:676–682. <https://doi.org/10.1038/nmeth.2019>
 34. Wagner CD, Davis LE, Zeller MV et al (1981) Empirical atomic sensitivity factors for quantitative analysis by electron spectroscopy for chemical analysis. *Surf Interface Anal* 3:211–225. <https://doi.org/10.1002/sia.740030506>
 35. Magalhães JL, Moreira LM, Rodrigues-Filho UP et al (2002) Surface chemistry of the iron tetraazamacrocyclic on the aminopropyl-modified surface of oxidized n-Si(100) by AFM and XPS. *Surf Interface Anal* 33:293–298. <https://doi.org/10.1002/sia.1186>
 36. Scofield JH (1976) Hartree-Slater subshell photoionization cross-sections at 1254 and 1487 eV. *J Electron SpectroscRelat Phenomena* 8:129–137. [https://doi.org/10.1016/0368-2048\(76\)80015-1](https://doi.org/10.1016/0368-2048(76)80015-1)
 37. Zhao D, Huo Q, Feng J et al (1998) Nonionic triblock and star diblock copolymer and oligomeric surfactant syntheses of highly ordered, hydrothermally stable, mesoporous silica structures. *J Am ChemSoc* 120:6024–6036. <https://doi.org/10.1021/ja974025i>
 38. Rodríguez-Gómez A, Platero F, Caballero A, Colón G (2018) Improving the direct synthesis of hydrogen peroxide from hydrogen and oxygen over Au-Pd/SBA-15 catalysts by selective functionalization. *MolCatal* 445:142–151. <https://doi.org/10.1016/j.mcat.2017.10.034>
 39. Thommes M, Kaneko K, Neimark AV et al (2015) Physisorption of gases, with special reference to the evaluation of surface area and pore size distribution (IUPAC Technical Report). *Pure ApplChem* 87:1051–1069. <https://doi.org/10.1515/pac-2014-1117>
 40. Choma J, Jaroniec M (2007) Applicability of classical methods of pore size analysis for MCM-41 and SBA-15 silicas. *Appl Surf Sci* 253:5587–5590. <https://doi.org/10.1016/j.apsusc.2006.12.059>
 41. Luz GE, Lima SH, Melo ACR et al (2010) Direct synthesis and characterization of LaSBA-15 mesoporous molecular sieves. *J Mater Sci* 45:1117–1122. <https://doi.org/10.1007/s10853-009-4054-y>
 42. Meynen V, Cool P, Vansant EF (2009) Verified syntheses of mesoporous materials. *Microporous Mesoporous Mater* 125:170–223. <https://doi.org/10.1016/j.micromeso.2009.03.046>
 43. Ma Z, Dai S (2011) Development of novel supported gold catalysts: a materials perspective. *Nano Res* 4:3–32. <https://doi.org/10.1007/s12274-010-0025-5>
 44. Gutiérrez LF, Hamoudi S, Belkacemi K (2011) Synthesis of gold catalysts supported on mesoporous silica materials: recent developments. *Catalysts* 1(1):97–154
 45. Kučerová G, Strunk J, Muhler M, Behm RJ (2017) Effect of Titania surface modification of mesoporous silica SBA-15 supported Au catalysts: activity and stability in the CO oxidation reaction. *J Catal* 356:214–228. <https://doi.org/10.1016/j.jcat.2017.09.017>
 46. Katiyar A, Ji L, Smirniotis P, Pinto NG (2005) Protein adsorption on the mesoporous molecular sieve silicate SBA-15: effects of pH and pore size. *J Chromatogr A* 1069:119–126. <https://doi.org/10.1016/j.chroma.2004.10.077>
 47. Benamor T, Vidal L, Lebeau B, Marichal C (2012) Influence of synthesis parameters on the physico-chemical characteristics of SBA-15 type ordered mesoporous silica. *Microporous Mesoporous Mater* 153:100–114. <https://doi.org/10.1016/j.micromeso.2011.12.016>
 48. Tiruvalam RC, Pritchard JC, Dimitratos N et al (2011) Aberration corrected analytical electron microscopy studies of sol-immobilized Au + Pd, Au{Pd} and Pd{Au} catalysts used for benzyl alcohol oxidation and hydrogen peroxide production. *Faraday Discuss* 152:63. <https://doi.org/10.1039/c1fd00020a>
 49. Odio OF, Lartundo-Rojas L, Santiago-Jacinto P et al (2014) Sorption of gold by naked and thiol-capped magnetite nanoparticles: an XPS approach. *J PhysChem C* 118:2776–2791. <https://doi.org/10.1021/jp409653t>
 50. Guo S, Zhang S, Fang Q et al (2018) Gold-palladium nanoalloys supported by graphene oxide and lamellar TiO₂ for direct synthesis of hydrogen peroxide. *ACS Appl Mater Interfaces* 10:40599–40607. <https://doi.org/10.1021/acsami.8b17342>
 51. SiavashMoakhar R, Jalali M, Kushwaha A et al (2018) AuPd bimetallic nanoparticle decorated TiO₂ rutile nanorod arrays for enhanced photoelectrochemical water splitting. *J ApplElectrochem* 48:995–1007. <https://doi.org/10.1007/s10800-018-1231-1>
 52. Bharti B, Kumar S, Lee H-N, Kumar R (2016) Formation of oxygen vacancies and Ti³⁺ state in TiO₂ thin film and enhanced optical properties by air plasma treatment. *Sci Rep* 6:32355. <https://doi.org/10.1038/srep32355>
 53. Sanjinés R, Tang H, Berger H et al (1994) Electronic structure of anatase TiO₂ oxide. *J ApplPhys* 75:2945–2951. <https://doi.org/10.1063/1.356190>
 54. Chenakin SP, Melaet G, Szukiewicz R, Kruse N (2014) XPS study of the surface chemical state of a Pd/(SiO₂+TiO₂) catalyst after methane oxidation and SO₂ treatment. *J Catal* 312:1–11. <https://doi.org/10.1016/j.jcat.2014.01.008>
 55. Paparazzo E, Fanfoni M, Severini E, Priori S (1992) Evidence of Si–OH species at the surface of aged silica. *J VacSciTechnol A* 10:2892–2896. <https://doi.org/10.1116/1.577726>
 56. Post P, Wurlitzer L, Maus-Friedrichs W, Weber A (2018) Characterization and applications of nanoparticles modified in-flight with silica or silica-organic coatings. *Nanomaterials* 8:530. <https://doi.org/10.3390/nano8070530>
 57. Wang Z-L, Yan J-M, Ping Y et al (2013) An efficient CoAuPd/C catalyst for hydrogen generation from formic acid at room

- temperature. *AngewChemieInt Ed* 52:4406–4409. <https://doi.org/10.1002/anie.201301009>
58. Qian K, Huang W (2011) Au–Pd alloying-promoted thermal decomposition of PdO supported on SiO₂ and its effect on the catalytic performance in CO oxidation. *Catal Today* 164:320–324. <https://doi.org/10.1016/j.cattod.2010.10.018>
 59. Venezia A (2003) Activity of SiO₂ supported gold-palladium catalysts in CO oxidation. *ApplCatal A Gen* 251:359–368. [https://doi.org/10.1016/S0926-860X\(03\)00343-0](https://doi.org/10.1016/S0926-860X(03)00343-0)
 60. Malkhasian AYS, Narasimharao K (2017) Structural and photocatalytic properties of Pd-deposited semiconductors with different morphology. *RSC Adv* 7:55633–55645. <https://doi.org/10.1039/C7RA11080D>
 61. Wang S, Zhao Q, Wei H et al (2013) Aggregation-free gold nanoparticles in ordered mesoporous carbons: toward highly active and stable heterogeneous catalysts. *J Am Chem Soc* 135:11849–11860. <https://doi.org/10.1021/ja403822d>
 62. Savara A, Chan-Thaw CE, Sutton JE et al (2017) Molecular origin of the selectivity differences between palladium and gold-palladium in benzyl alcohol oxidation: different oxygen adsorption properties. *ChemCatChem* 9:253–257. <https://doi.org/10.1002/cctc.201601295>
 63. Enache DI, Knight DW, Hutchings GJ (2005) Solvent-free oxidation of primary alcohols to aldehydes using supported gold catalysts. *Catal Lett* 103:43–52. <https://doi.org/10.1007/s10562-005-6501-y>
 64. Jiang Y, Chen M, Yang Y et al (2018) Facile synthesis of AuPd nanoparticles anchored on TiO₂ nanosheets for efficient dehydrogenation of formic acid. *Nanotechnology*. <https://doi.org/10.1088/1361-6528/aac79e>
 65. Cao E, Sankar M, Nowicka E et al (2013) Selective suppression of disproportionation reaction in solvent-less benzyl alcohol oxidation catalysed by supported Au–Pd nanoparticles. *Catal Today* 203:146–152. <https://doi.org/10.1016/j.cattod.2012.05.023>
 66. Cao E, Sankar M, Firth S et al (2011) Reaction and Raman spectroscopic studies of alcohol oxidation on gold-palladium catalysts in microstructured reactors. *ChemEng J* 167:734–743. <https://doi.org/10.1016/j.cej.2010.08.082>
 67. Wang D, Villa A, Porta F et al (2008) Bimetallic gold/palladium catalysts: correlation between nanostructure and synergistic effects. *J PhysChem C* 112:8617–8622. <https://doi.org/10.1021/jp800805e>
 68. Abad A, Almela C, Corma A, García H (2006) Efficient chemoselective alcohol oxidation using oxygen as oxidant. Superior performance of gold over palladium catalysts. *Tetrahedron* 62:6666–6672. <https://doi.org/10.1016/j.tet.2006.01.118>

Publisher's Note Springer Nature remains neutral with regard to jurisdictional claims in published maps and institutional affiliations.

Authors and Affiliations

Jussara Morais da Silva¹ · Renilma Carvalho Sousa¹ · Jean Cláudio S. Costa¹ · Janildo Lopes Magalhães¹ · Geraldo E. Luz Jr.² · Carla Veronica Rodarte de Moura¹ · Edmilson Miranda de Moura¹ 

¹ Chemistry Department, Federal University of Piauí, Teresina, PI 64049-550, Brazil

² PPGQ-DQ, State University of Piauí-UESPI, Teresina, PI 64002-150, Brazil